Modeling of a Superconducting Radial Flux Inductor by a 3D Reluctance Network

Moussa Kelouaz, Youcef Ouazir, Larbi Hadjout, Smail Mezani, Thierry Lubin, Kévin Berger, Jean Lévêque

Modeling of a Superconducting Radial Flux Inductor by a 3D Reluctance Network

1st Moussa KELOUAZ
LSEI.
Université des Sciences et de la Technologie Houari Boumediene
Algiers, Algeria
mkelouaz@usthb.dz

2nd Youcef OUAZIR
LSEI.
Université des Sciences et de la Technologie Houari Boumediene
Algiers, Algeria
youazir@yahoo.fr

3rd Larbi HADJOUT
LSEI.
Université des Sciences et de la Technologie Houari Boumediene
Algiers, Algeria
lhajdout@yahoo.fr

4th Smaïl MEZANI
GREEN
Université de Lorraine, Faculté des Sciences et Technologies
Vandœuvre-lès-Nancy, France
smail.mezani@univ-lorraine.fr

5th Thierry LUBIN
GREEN
Université de Lorraine, Faculté des Sciences et Technologies
Vandœuvre-lès-Nancy, France
thierry.lubin@univ-lorraine.fr

6th Kévin BERGER
GREEN
Université de Lorraine, Faculté des Sciences et Technologies
Vandœuvre-lès-Nancy, France
kevin.berger@univ-lorraine.fr

7th Jean LÉVÊQUE
GREEN
Université de Lorraine, Faculté des Sciences et Technologies
Vandœuvre-lès-Nancy, France
jean.leveque@univ-lorraine.fr

***Abstract*— In this paper we present a quick 3D model using reluctance network (RN) of a radial flux superconducting inductor dedicated to a synchronous machine. This inductor is made of two kinds of superconducting materials; two NbTi coaxial coils fed by currents in opposite directions and four rectangular YBCO pieces placed between the two coils to modulate the generated magnetic field. This inductor is fed by 260 A and cooled at 4.2 K. Flux densities computed by the 3D RN are compared to FE simulations and to experiments.**

Keywords—Reluctance network, superconducting inductor, superconducting synchronous machine.

I. Introduction

The use of superconducting (SC) materials led to a variety of inductor topologies dedicated to synchronous machines (radial, axial, homopolar…). These topologies are proposed to improve the power density of electrical machines by taking advantage of SC windings to produce high magnetic fields and SC bulks for their capability of screening strong magnetic fields. Based on these two properties of SC materials, two prototypes of radial flux SC synchronous machines have been constructed and successfully tested; the first one is based on "flux concentration" [1]-[2] and the second one is based on "flux deviation" [3]. The electromagnetic field computation of these two machines uses 3D finite elements which provide precise results, but the computation time is high.

We present in this paper a 3D reluctance network (RN) of the "flux concentration" inductor realized and tested in GREEN laboratory [1]. The motivation of developing a full 3D RN model is to get more precise results than the simplified 2D model described in [4] and to reduce the cpu time inherent to the use of 3D finite elements. The 3D RN approach has been successfully used for the "flux deviation inductor" [5].

II. Description of the Supercodncuting Inductor

The studied SC inductor is shown in Fig.1. It consists of two SC solenoids and four rectangular SC bulks which have a diamagnetic behavior under zero-field cooling. The bulks act as screens to the magnetic field created by two solenoids supplied by dc currents in contra-directions. The obtained airgap field is multipolar as in conventional ac machines. The flux density is minimal above a SC bulk and maximal above the bulks interspaces. For the studied inductor, this "flux concentration" results in 8 poles.

The studied inductor has been realized and tested [1]. It has been placed in a cryostat and cooled in liquid helium at a temperature of 4.2 K. The two coils are powered by opposite dc currents of 260 A. The main parameters and characteristics of this inductor are shown in Fig.2 and Tab.1.

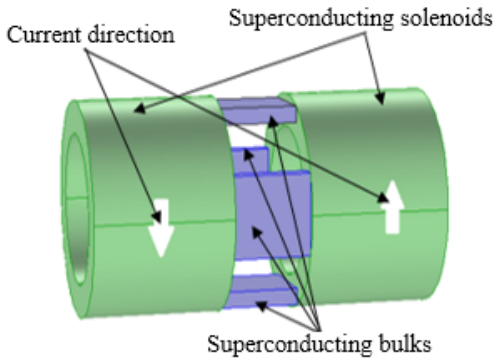

Fig.1. 3D view of the studied superconducting inductor.

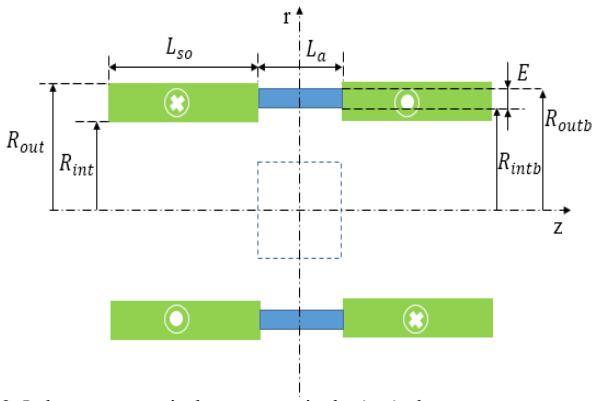

Fig. 2. Inductor geometrical parameters in the (r, z) plan.

Tab.1 Main parameters of the studied inductor.

Symbol	Designation	Value	Units
NbTi	Solenoid wire material	-	-
d_w	NbTi round wire diameter	0.7	mm
R_{out}	Solenoids outer radius	33	mm
R_{int}	Solenoids inner radius	23	mm
L_a	Distance between solenoids	25	mm
L_{so}	Length of the solenoid	45	mm
YBCO	SC bulk material	-	-
R_{outb}	SC bulk outer radius	31	-
R_{intb}	SC bulk inner radius	26	-
E	Thickness of the SC bulk	5	mm

III. Finite Element Analysis

The determination of the magnetic field in the studied structure is typically a 3D problem. The symmetry of the problem allows us to reduce the study domain to a pole-pair of the inductor with periodicity conditions, Fig.3. In addition, only half the inductor is considered in the axial direction.

Two FE calculation models are developed: the first one uses a magnetic vector potential formulation and the second one a magnetic scalar potential formulation. The second one is faster (one variable V against three for the vector potential A), but we need to replace the solenoid by an equivalent magnet using a Coulombian model [6].

If J is the ortho-radial current density in the solenoid, its equivalent magnet is then characterized by two magnetizations $\overrightarrow{M_1}$ and $\overrightarrow{M_2}$ in the z direction (Fig.4):

$$\overrightarrow{M_1} = (R_{out} - R_{\text{int}}).J\overrightarrow{u_z} \quad , 0 \le r < R_{\text{int}} \tag{1}$$

$$\overrightarrow{M_2} = (R_{out} - r).J\overrightarrow{u_z} \quad , R_{\text{int}} \le r \le R_{out} \tag{2}$$

It has to be noted that a diamagnetic like model is used for the SC bulk to mimics its shielding properties. Hence, the relative permeability of the SC bulk is set to 10^{-3}.

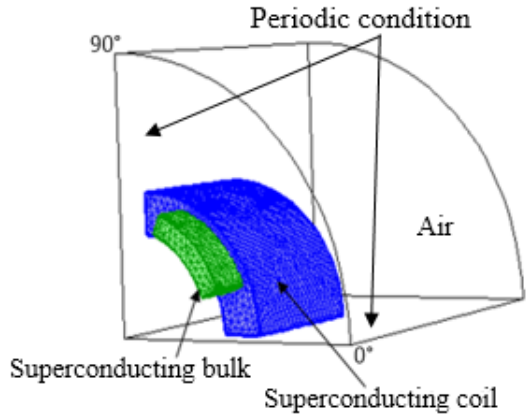

Fig.3. 3D FE model of 1 pole-pair with the mesh of the active parts

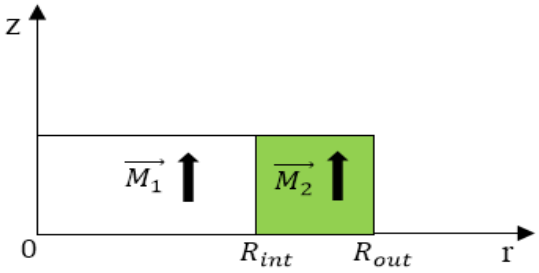

Fig.4. Representation of a coil by an equivalent magnet.

IV. Reluctance Network Model

A meshed reluctance network method is used here to model, in 3D, the studied SC inductor.

This method consists of meshing the geometry by dividing it into a set of volume elements with a given geometric form [7]-[10]. As for the finite element method, each generated volume element represents a material node characterized by:

- a constant permeability
- reluctances in the different directions
- mmfs if the volume element is in the region of field source.

The different material nodes are then connected through their reluctances in all directions. The application of Kirchhoff's laws to the obtained reluctance network leads to an algebraic system of equations. The resolution of this system gives the nodal values of the magnetic potential from which we can derive the flux density distribution and the fluxes.

A. 3D model of a base element

To mesh the complex geometry of the studied inductor, we perform a cut in cylindrical coordinates (longitudinal z, radial r and ortho-radial θ). Hence, the volume element has the form of a hollow cylinder sector shown in Fig. 5. To calculate the three components of the magnetic field in the volume element mesh of Fig.6, one must know all the magnetic and geometric properties of the elements. This element is modeled by six reluctances (two per direction) leading to six peripheral nodes connected to the adjacent elements.

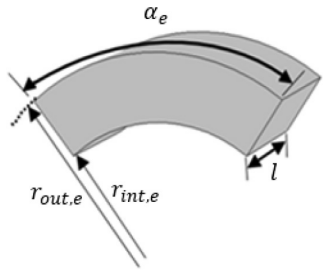

Fig. 5. 3D hollow cylinder sector element.

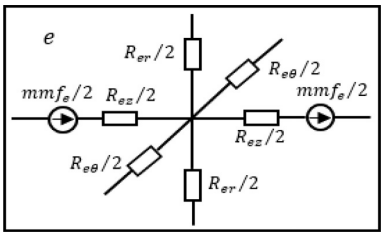

Fig. 6. 3D model of active element (with mmf).

All reluctances are connected to the central node (material node) representing this element (Fig.6). In addition, the source of the magnetic field is represented by an m.m.f in series with reluctances in the appropriate directions. An element without mmf is said "passive", otherwise it is said "active".

The reluctances R_r , R_θ , R_z in radial, ortho-radial and longitudinal directions respectively are calculated by [5]:

$$R_{er} = \frac{1}{\alpha_e \mu_e l} ln \frac{r_{out,e}}{r_{int,e}} \tag{3}$$

in the radial direction (r),

$$R_{e\theta} = \frac{\alpha_e}{\mu_e l} \frac{1}{ln \frac{r_{out,e}}{r_{int,e}}} \tag{4}$$

in the ortho-radial direction (θ) and

$$R_{ez} = \frac{2l}{\mu_e \alpha_e \left(\left(r_{out,e} \right)^2 - \left(r_{int,e} \right)^2 \right)} \tag{5}$$

in the longitudinal direction (z).

μ_e , α_e , $r_{out,e}$, $r_{int,e}$, l are respectively the permeability, the opening angle, the outer radius, the inner radius and the axial length of element. The expression of the MMF in the center of the mesh element in the coil region is then:

$$F_e = \begin{cases} F_{emax} \quad , \quad \text{if } r < R_{int} \\ F_{emax} \left(1 - \left(\dfrac{\left(r_{out,e} - r_{int,e} \right)}{2} + \left(r_{int,e} - R_{int} \right) \right) \right) , \text{if } R_{\text{int}} \le r < R_{out} \end{cases} \tag{6}$$

$$F_{emax} = L_{so} \left(R_{out} - R_{int} \right) J \tag{7}$$

where J , L_{so} , R_{out} and R_{int} are the ortho-radial current density in the coil, the length, the outer and inner radius of the coil respectively.

B. Equations of a 3D element

In the element reluctance network of Fig. 6, the magnetic potential at the center of the element (material node) is noted u_e and those at the connection nodes with the adjacent elements are noted (u_{1r}, u_{2r}), ($u_{1\theta}$, $u_{2\theta}$) and (u_{1z}, u_{2z}). These potentials are directly linked to the branches defined by the reluctances (R_{1r}, R_{2r}), ($R_{1\theta}$, $R_{2\theta}$) and (R_{1z}, R_{2z}). In a "passive" element, the relation between the magnetic potentials and the magnetic fluxes (φ_{1r}, φ_{2r}), ($\varphi_{1\theta}$, $\varphi_{2\theta}$) and (φ_{1z}, φ_{2z}), can be written as:

$$((R_{ir} + R_{er})/2)\varphi_{ir} = u_e - u_{ir} \qquad i = 1,2 \tag{8}$$

along the radial direction,

$$((R_{i\theta} + R_{e\theta})/2)\varphi_{i\theta} = u_e - u_{i\theta} \qquad i = 1,2 \tag{9}$$

along the ortho-radial direction and

$$((R_{iz} + R_{ez})/2)\varphi_{iz} = u_e - u_{iz} \qquad i = 1,2 \tag{10}$$

along the longitudinal direction.

For an "active" element having mmfs given by (6), we can write:

$$((R_{iz} + R_{ez})/2)\varphi_{iz} = u_e - u_{iz} - mmf_e/2 \qquad i = 1,2 \tag{11}$$

Moreover, the magnetic flux conservation in the element leads to:

$$\sum_{i=1}^{2} \varphi_{ir} + \varphi_{i\theta} + \varphi_{iz} = 0 \tag{12}$$

C. Global system of equations

Rewriting equations (8)-(11) allows the determination of the magnetic fluxes (φ_{1r}, φ_{2r}), ($\varphi_{1\theta}$, $\varphi_{2\theta}$) and (φ_{1z}, φ_{2z}) expressions as a function of the permeances (inverse of the reluctances) and the mmfs. Replacing these expressions in (12) leads to a relation between the mmfs (F_e for active element and 0 for passive one) and the magnetic potential. Furthermore, 6 extra equations are determined using the continuity of the flux at a connection node of 2 adjacent elements. From the former relations, one can establish an algebraic system of equations whose unknowns are the magnetic potentials at the nodes of the mesh. This system is written in matrix form as:

$$[\mathrm{P}]\{U\} = \{\mathrm{F}_s\} \tag{13}$$

where [P], $\{U\}$ and $\{F_s\}$, are respectively the permeance matrix, the vector of nodal values of the magnetic potential and the vector of flux sources.
The matrix [P] is constant as we consider a linear case in this study. For the resolution of (13), a null potential is imposed in a reference node.
The resolution of (13) gives the distribution of the magnetic potential in all material nodes of the 3D mesh. The electromagnetic characteristics of the studied inductor are then computed with these nodal values.

For an elements (*e*) having a cross section S_e along a given direction (radial, orthoradial or longitudinal), the flux density is determined using the flux through the branch which connects element *(e)* to its adjacent element *(k)* in the considered direction. It is computed by:

$$B_e(r,\theta,z) = \frac{\varphi_{ek}}{S_e} \tag{14}$$

where φ_{ek} the flux through the branches connecting elements *(e)* and *(k)*:

$$\varphi_{ek} = \frac{(U_k - U_e)}{R_{ek}} \tag{15}$$

R_{ek} is the equivalent reluctance of the considered branch.

V. Resuls

The studied SC inductor having parameters given in Tab.1 is tested and computed by the developed RN and FE models. The coils are powered by opposite currents of 260 A.

The SC bulk in the constructed inductor [1] is rectangular (Fig.7.a.) because it is difficult to practically get a sector shape. The RN model is developed in cylindrical coordinates, so it is necessary to replace the rectangular bulk by an equivalent sector one. In this study, we choose an equivalent sector bulk with the same cross section and thickness as the rectangular one (Fig.7.b.).

In order to experimentally check the RN and FE models, 10 Hall probes (S1 to S10) has been glued on the inductor surface R_{out} at z=0 to measure the radial flux density (Fig.7.a.).

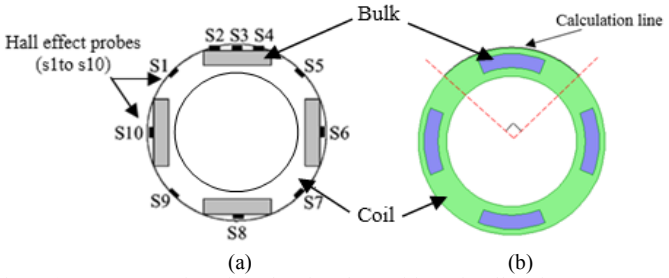

Fig.7. a) 2D cross section view showing the position of Hall probes [1]
b) calculation line and approximative sector shape of the bulks.

Two FE models are developed, one with the actual rectangular bulk and the other with the equivalent cylindrical sector bulk.

In Fig.8, the radial flux density component obtained by the two 3D FE and the RN models are compared to the measured one (the computations are taken on the circle drawn on Fig.7.b). As expected, the FE model with rectangular bulk gives results close to the measurements. The FE and RN models (with sector bulk) give almost the same results but are relatively far from the measurements, especially on the bulk surface (probes S2 to S4).

In Fig.9, the radial flux density waveform is plotted on a circle whose radius is equal to the inductor surface radius R_{out} plus 5mm at z=La/4 (see Fig.2 for the z location). The results are very similar as the relative difference doesn't exceed 5% between the 3 models in use.

The results of Figs. 8 and 9 show that the RN model (equivalent sector bulk) fails to accurately evaluate the magnetic field at the vicinity of the actual rectangular bulk. However, when the distance from the bulk increases, the RN model gives reliable results, so the bulk shape has less influence.

To test the accuracy and rapidity of the RN model, the flux density waveform is plotted in Fig.10 for 3 mesh densities consisting of 8640, 5760 and 2880 nodes respectively. FE computations (sector shape bulk) which use the magnetic vector and scalar potential formulations are also performed and give almost the same results. Compared to the FE simulations, the RN model gives very good results even for the coarsest mesh.

The corresponding cpu times are shown on Table 2. The RN model is clearly faster than the FE model with scalar potential even for the finest mesh of 8640 nodes used in study case 1. It has to be noted that the FE mesh is refined until convergent results are obtained.

VI. Conclusion

In this work, a 3D accurate and quick mesh-based reluctance network model is developed to compute the magnetic field distribution in a superconducting radial flux inductor. The computation time of this model is very low compared to the popular FE model. Hence, this model can be used as a fast tool for rapid scaling and optimization of this superconducting inductor's topology.

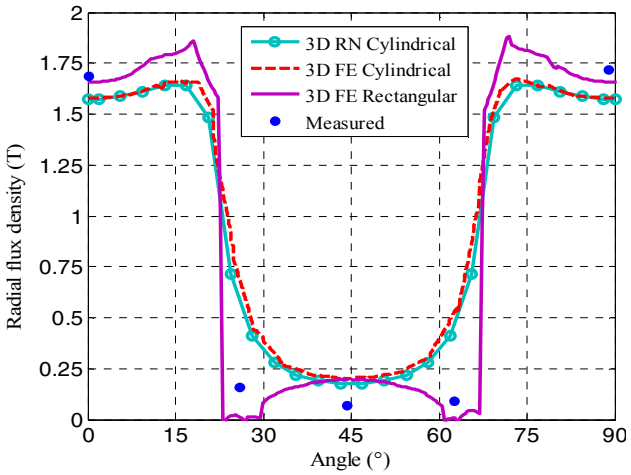

Fig.8. Radial flux density at r= Rout and z=0

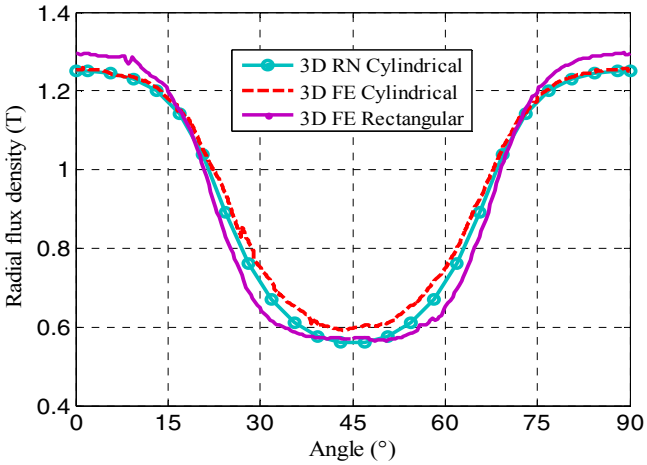

Fig.9. Radial flux density at r= Rout+5mm and z =La/4.

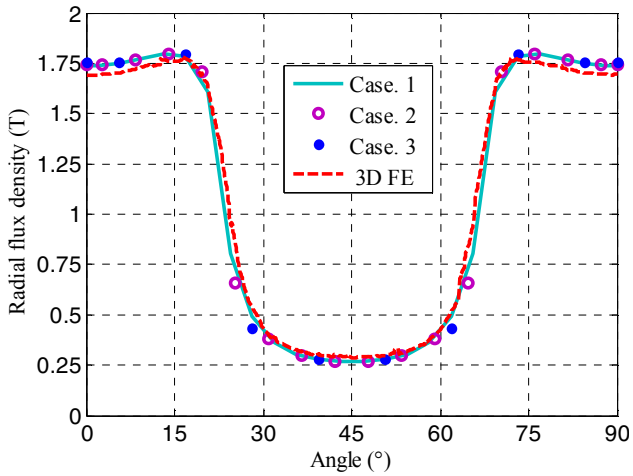

Fig.10. Radial flux density at r = R_{out} and z =La/4 for different RN meshes

Tab.2. Comparison of cpu times

	Number of nodes	cpu time (s)
RN, Case. 1	8640	5.31
RN, Case. 2	5760	1.74
RN, Case. 3	2880	0.47
FE, vector potential	216011	40
FE, scalar potential	216011	10

VII. References

[1] P. J. Masson, J. Leveque, D. Netter, and A. Rezzoug, "Experimental study of a new kind of superconducting inductor," *IEEE Trans. Appl. Supercond.*, vol. 13, no. 2, Jun. 2003, pp. 2239–2242.

[2] E. Ailam, D. Netter, J. Leveque, B. Douine, P.J. Masson, and A. Rezzoug, "Design and testing of a superconducting rotating machine," *IEEE Trans. Appl. Supercond.*, vol. 17, no. 1, March 2007, pp. 27–33.

[3] R. Alhasan, T. Lubin, B. Douine, Z.M. Adilov, and J. Lévêque, "Test of an original superconducting synchronous machine based on magnetic shielding," *IEEE Trans. Appl. Supercond.*, vol. 26, no. 4, Jun. 2016, pp. 1–5.

[4] G. Malé, S. Mezani, T. Lubin, and J. Leveque, "A fast analytical method to compute the radial flux density distribution in the airgap of a superconducting inductor," *IEEE Trans. Appl. Supercond.,* vol. 21, no. 3, Jun. 2011, pp. 1114 – 1118.

[5] M. Kelouaz and al., "3D Magnetic field modeling of a new superconducting synchronous machine using reluctance network method," *Phys. C: Supercond. Its Appl.,* vol. 548, May 2018, pp. 5–13.

[6] E. Durand, *Magnétostatiqe*, Ed. Masson et Cie, 1968, 675 p.

[7] V. Ostovic, *Dynamics of Saturated Electric Machines*, Springer-Verlag, New York, 1989, 445 p.

[8] B. Nedjar, S. Hlioui, L. Vido, Y. Amara, and M. Gabsi, "Hybrid Excitation Synchronous Machine Modeling Using Magnetic Equivalent Circuits," *International Conference on Electrical Machines (ICEM)*, Sept. 2011, Beijing, China.

[9] H. W. Derbas, J. M. Williams, A. C. Koenig, and S. D. Pekarek, "A Comparison of Nodal and Mesh-Based Magnetic Equivalent Circuit Models," *IEEE Trans. Ener. Conv.,* vol. 24, no. 2, pp.388-396, Jun. 2009.

[10] M. L. Bash, J. M. Williams, and S. D. Pekarek, "Incorporating Motion in Mesh-Based Magnetic Equivalent Circuits," *IEEE Trans. Ener. Conv.,* vol. 25, no. 2, pp.329-338, Jun. 2010.